Metal–Nitroxyl Interactions. 39. Electron–Electron Spin–Spin Splitting in the EPR Spectra of Nitroxyl Spin-Labeled Mn(II) Complexes in Fluid Solution

Jyoti K. More, Kundalika M. More, Gareth R. Eaton,* and Sandra S. Eaton

Contribution from the Departments of Chemistry, University of Denver, Denver, Colorado 80208, and University of Colorado at Denver, Denver, Colorado 80202. *Received December 15, 1983*

Abstract: X-band and Q-band EPR spectra have been obtained for a series of spin-labeled ligands coordinated to bis(hexafluoroacetylacetonato)manganese(II) and bis(trifluoroacetylacetonato)manganese(II) in fluid solution. Values of the exchange coupling constant, J, were obtained by computer simulation of the spectra and ranged from 14×10^{-4} to $>200 \times 10^{-4}$ cm^{-1}. Comparison of the values of J for these complexes with values obtained previously for the same ligands coordinated to VO(IV) indicate that J is about an order of magnitude smaller for Mn(II) which has $S = {}^5/_2$ than for VO(IV) which has $S = {}^1/_2$. The observation of spin–spin splitting indicates that the Mn(II) electron spin relaxation rate is slow relative to the magnitude of the spin–spin splitting.

We have observed electron–electron splitting in fluid solution EPR spectra of spin-labeled complexes of the $S = {}^1/_2$ metals VO(IV),[1-3] Cu(II),[1-6] and Ag(II).[1] A prerequisite for the observation of spin–spin splitting in the EPR spectra of spin-labeled metal complexes is that the metal relaxation rate must be slow relative to the magnitude of the splitting caused by the spin–spin interaction. Otherwise the metal electron spin relaxation would cause a collapse of the splitting. Metals with $S > {}^1/_2$ generally have faster relaxation rates than metals with $S = {}^1/_2$. It was therefore of interest to determine whether spin–spin splitting could be observed for metals with $S > {}^1/_2$. Mn(II) is of particular interest because of the widespread use of the model proposed by Leigh[7] for the analysis of spin–spin interaction between Mn(II) and nitroxyl spin-labels in biological molecules.[8] An essential assumption of the model is that the Mn(II) relaxation rate is fast relative to the magnitude of the spin–spin interaction and therefore that an increase in the metal relaxation rate (decrease in the relaxation time) would result in a narrowing of the EPR signal for an interacting organic radical.

The study of spin-labeled Mn(II) complexes is important for a second reason. In two series of homonuclear metal dimers the antiferromagnetic exchange interaction decreased as the metal was varied along the series Cu(II), Ni(II), Co(II), Fe(II), and Mn(II).[9,10] In heteronuclear Cu(II)–M(II) dimers (M = Cu(II), Ni(II), Co(II), Fe(II), Mn(II)) the exchange interaction decreased similarly.[11-13] One report suggested that the changes in the interaction were due to structural changes in the dimers.[12] Other authors have suggested that the decrease was due to the increase in the number of unpaired electrons on the metal.[9,13] If that explanation is correct, a similar decrease in the exchange interaction would be expected for a spin-labeled Mn(II) complex compared to an analogous spin-labeled Cu(II) or VO(IV) complex.

In this paper we report the analysis of the fluid solution EPR spectra of spin-labeled ligands I–XII coordinated to bis(trifluoroacetylacetonato)manganese(II) ($Mn(tfac)_2$) and bis(hexafluoroacetylacetonato)manganese(II) ($Mn(hfac)_2$). The EPR spectra of I–XI coordinated to bis(hexafluoroacetylacetonato)copper(II)[2,3,14,15] and of I, II, IV, V, VIII, IX, X, and XI coordinated to bis(trifluoroacetylacetonato)oxovanadium(IV) and bis(hexafluoroacetylacetonato)oxovanadium(IV)[2,3] have been reported.

Experimental Section

Physical Measurements. Infrared spectra were obtained in halocarbon mulls on a Perkin-Elmer 283B spectrometer. X-band EPR spectra were obtained on a Varian E-9 spectrometer. The spectrometer used for the Q-band EPR spectra has been described.[16] The solutions used to obtain the EPR spectra were about 2×10^{-3} M. The lines in the spectra were sufficiently broad that the line widths were unchanged by removal of oxygen. Therefore most of the spectra were run on solutions which were air saturated. All spectra were obtained at microwave powers well below

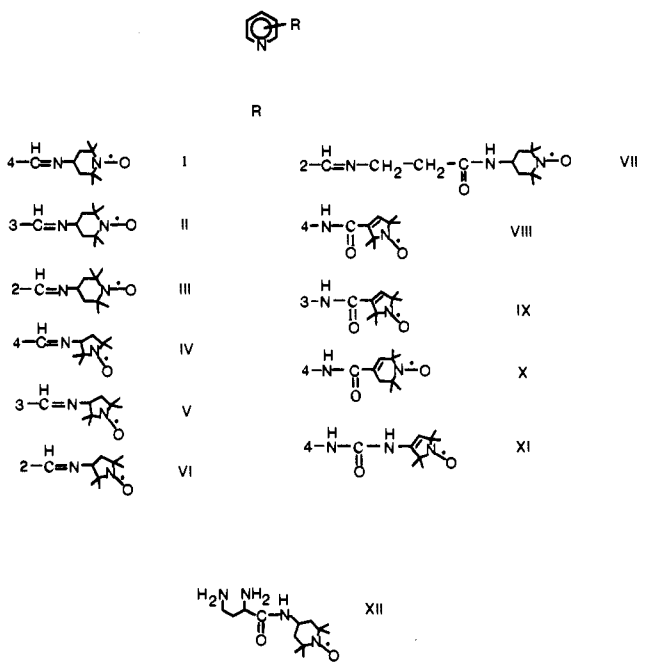

* University of Denver.

(1) More, K. M.; Eaton, S. S.; Eaton, G. R. *J. Am. Chem. Soc.* **1981**, *103*, 1087–1090.
(2) Sawant, B. M.; Shroyer, A. L. W.; Eaton, G. R.; Eaton, S. S. *Inorg. Chem.* **1982**, *21*, 1093–1101.
(3) More, J. K.; More, K. M.; Eaton, G. R. Eaton, S. S. *Inorg. Chem.* **1982**, *21*, 2455–2460.
(4) Sawant, B. M.; Braden, G. A.; Smith, R. E.; Eaton, G. R.; Eaton, S. S. *Inorg. Chem.* **1981**, *20*, 3349–3354.
(5) More, K. M.; Sawant, B. M.; Eaton, G. R.; Eaton, S. S. *Inorg. Chem.* **1981**, *20*, 3354–3362.
(6) More, K. M.; Eaton, G. R.; Eaton. S. S. *Can. J. Chem.* **1982**, *60*, 1392–1401 and references therein.
(7) Leigh, J. S., Jr. *J. Chem. Phys.* **1970**, *52*, 2608–2612.
(8) Eaton, G. R.; Eaton, S. S. *Coord. Chem. Rev.* **1978**, *26*, 207–262.
(9) Lambert, S. L.; Hendrickson, D. N. *Inorg. Chem.* **1979**, *18*, 2683–2686.
(10) Spiro, C. L.; Lambert, S. L.; Smith, T. J.; Duesler, E. N.; Gagne, R. P.; Hendrickson, D. N. *Inorg. Chem.* **1981**, *20*, 1229–1237.
(11) Torihara, N.; Okawa, H.; Kida, S. *Chem. Lett.* **1978**, 185–188.
(12) O'Conner, C. J.; Freberg, D. P.; Sinn, E. *Inorg. Chem.* **1979**, *18*, 1077–1088.
(13) Lambert, S. L.; Spiro, C. L.; Gagne, R. R.; Hendrickson, D. H. *Inorg. Chem.* **1982**, *21*, 68–72.
(14) Boymel, P. M.; Eaton, G. R.; Eaton, S. S. *Inorg. Chem.* **1980**, *19*, 727–735.
(15) Boymel, P. M.; Braden, G. A.; Eaton, G. R.; Eaton, S. S. *Inorg. Chem.* **1980**, *19*, 735–739.

0002-7863/84/1506-5395$01.50/0

saturation and at modulation amplitudes which did not cause distortion of the line shapes. Elemental analyses were performed by Spang Microanalytical Laboratory.

Preparation of Compounds. The following compounds were prepared by literature methods: I–III,[14] IV–VI,[15] VIII–X,[2] XI,[3] XII,[17] Mn(tfac)$_2$,[18,19] Mn(hfac)$_2$·2H$_2$O.[18,20]

***N*-(2,2,6,6-Tetramethyl-1-oxy-4-piperidinyl)-3-(trifluoroacetamido)propionamide (XIII).** Dry triethylamine (0.30 g, 3.0 mmol) was added to a stirred solution of 3-(trifluoroacetamido)propionic acid[21] (0.555 g, 3.0 mmol) in 20 mL of dry diethyl ether under nitrogen. The solution was cooled in an ice bath, and a solution of ethyl chloroformate (0.33 g, 3.0 mmol) in 10 mL of dry diethyl ether was added dropwise over a period of 15 min. The solution was brought to room temperature and stirred for 2 hr. The solution was filtered and cooled in an ice bath. A solution of 4-amino-2,2,6,6-tetramethylpiperidinyl-1-oxy (0.516 g, 3.0 mmol) in 10 mL of dry diethyl ether was added dropwise. The solution was refluxed for 12 h. The solvent was removed, and the residue was dissolved in 200 mL of dichloromethane. The solution was washed with 0.1 N HCl (300 mL) and saturated aqueous sodium bicarbonate (200 mL). The dichloromethane solution was dried over Na_2SO_4 and concentrated to give a red oil which crystallized upon addition of 2 mL of diethyl ether. The solid was purified by chromatography on silica gel in chloroform solution and recrystallized from diethyl ether: yield, 0.65 g, 64%, yellow solid; mp 128 °C; IR 3200 (NH), 3300 (NH), 1720 (C=O), 1660 (C=O) cm^{-1}. Anal. Calcd for $C_{14}H_{23}N_3O_3F_3$: C, 49.70; H, 6.85; N, 12.42. Found: C, 49.89; H, 6.82; N, 12.48.

2-[((2-(((2,2,6,6-Tetramethyl-1-oxy-4-piperidinyl)amino)carbonyl)ethyl)imino)methyl]pyridine (VII). XIII (3.38 g, 1.0 mmol) was dissolved in a mixture of 25 mL of 1.0 N aqueous NaOH and 5 mL of 95% ethanol. The mixture was stirred for 2 h at room temperature and extracted with 300 mL of chloroform. The chloroform solution was dried over Na_2SO_4 and concentrated to give 3-amino-*N*-(2,2,6,6-tetramethyl-1-oxy-4-pyridinyl)propionamide as a yellow oil. The oil was dissolved in 20 mL of ethanol, and 2-pyridinecarboxaldehyde (0.107 g, 1.0 mmol) was added. The solution was refluxed for 2 h and the solvent was removed. The residue was crystallized from 1:1 ether:hexane to give a red solid: yield, 0.22 g, 66%; mp 112 °C; IR 3260 (NH), 1675 (C=O), 1645 (C=C) cm^{-1}. Anal. Calcd. for $C_{18}H_{27}N_4O_2$: C, 65.23; H, 8.21; N, 16.90. Found: C, 65.17; H, 8.28; N, 17.01.

Calculations

The Hamiltonian for the spin-labeled Mn(II) complexes in fluid solution is given in eq 1. The subscripts 1 and 2 refer to manganese and nitroxyl, respectively, J is the isotropic exchange coupling constant, and other symbols have their usual meanings. The

$$\mathcal{H} = \beta H(g_1S_1 + g_2S_2) + A_1S_1I_1 + A_2S_2I_2 + JS_1S_2 \quad (1)$$

spectra were analyzed by using a perturbation calculation in which the terms in eq 2 were treated exactly and the terms in eq 3 were treated to second order. The nitroxyl nitrogen hyperfine is

$$\mathcal{H}^0 = \beta H(g_1S_1 + g_2S_2) + A_1S_{1z}I_{1z} + A_2S_{2z}I_{2z} + JS_{1z}S_{2z} + \tfrac{1}{2}J(S_{1+}S_{2-} + S_{1-}S_{2+}) \quad (2)$$

$$\mathcal{H}' = \tfrac{1}{2}A_1(S_{1+}I_{1-} + S_{1-}I_{1+}) \quad (3)$$

sufficiently small in fluid solution that the corresponding second-order terms were neglected. The wave functions in the uncoupled representation are $|M_1, M_2, m_1, m_2\rangle$ where $M_1 = \pm^5/_2, \pm^3/_2, \pm^1/_2$, $M_2 = \pm^1/_2$, and m_1 and m_2 are the nuclear spin states of the manganese and nitroxyl nitrogen, respectively. $|^5/_2, {}^1/_2, m_1, m_2\rangle$ and $|{}^{-5}/_2, {}^{-1}/_2, m_1, m_2\rangle$ are eigenfunctions of the Hamiltonian in eq 2 and will subsequently be referred to as energy levels 1 and 12. The other ten wave functions for a particular combination of values of m_1 and m_2 give 2 × 2 matrices along the diagonal of the energy matrix. The matrices have the form given in eq 4 where $S_1(S_1 + 1) = 8.75$. Diagonalization of the 2 × 2 matrices gives the energy levels as in eq 5. The two wave

	$\lvert M_1, -\frac{1}{2}, m_1, m_2\rangle$	$\lvert M_1-1, \frac{1}{2}, m_1, m_2\rangle$
$\langle M_1, -\frac{1}{2}, m_1, m_2$	$\beta H(M_1g_1 - \frac{1}{2}g_2) + A_1M_1m_1 - \frac{1}{2}A_2m_2 - \frac{1}{2}J M_1$	$\frac{1}{2}J(8.75 - M_1(M_1-1))^{1/2}$
$\langle M_1-1, \frac{1}{2}, m_1, m_2$	$\frac{1}{2}J(8.75 - M_1(M_1-1))^{1/2}$	$\beta H((M_1-1)g_1 + \frac{1}{2}g_2) + A(M_1-1)m_1 + \frac{1}{2}A_2m_2 + \frac{1}{2}J(M_1-1)$

(4)

$$E_{n,n+1} = \mathrm{EF1}(M_1) \pm \mathrm{EF2}(M_1) \quad (5)$$

$$n = 7 - 2M_1$$

$$M_1 = 5/2, 3/2, 1/2, -1/2, -3/2$$

$$\mathrm{EF1}(M_1) = \beta H(M_1 - \tfrac{1}{2})g_1 + A_1m_1(M_1 - \tfrac{1}{2}) - \tfrac{1}{4}J$$

$$\mathrm{EF2}(M_1) = [\tfrac{1}{4}[\beta H(g_1 - g_2) + (A_1m_1 - A_2m_2) - J(M_1 - \tfrac{1}{2})]^2 + \tfrac{1}{4}J^2(8.75 - M_1(M_1-1))]^{1/2}$$

functions are given by eq 6 and 7.

$$\Psi n = -B(M_1)|M_1,-\tfrac{1}{2},m_1,m_2\rangle + C(M_1)|M_1 - 1,\tfrac{1}{2},m_1,m_2\rangle \quad (6)$$

$$\Psi n+1 = C(M_1)|M_1,-\tfrac{1}{2},m_1,m_2\rangle + B(M_1)|M_1 - 1,\tfrac{1}{2},m_1,m_2\rangle \quad (7)$$

The coefficients are defined as

$$\mathrm{NUM}(M_1) = -\tfrac{1}{2}\beta H(g_1 - g_2) - \tfrac{1}{2}(A_1m_1 - A_2m_2) + \tfrac{1}{2}J(M_1 - \tfrac{1}{2}) - \mathrm{EF2}(M_1)$$

$$\mathrm{DENOM}(M_1) = [(\mathrm{NUM}(M_1))^2 + \tfrac{1}{4}J^2 + \tfrac{1}{4}J^2(8.75 - M_1(M_1 - 1))]^{1/2}$$

$$B(M_1) = \frac{\mathrm{NUM}(M_1)}{\mathrm{DENOM}(M_1)}$$

$$C(M_1) = \frac{\tfrac{1}{2}J(8.75 - M_1(M_1 - 1))^{1/2}}{\mathrm{DENOM}(M_1)}$$

Due to the nature of the transitions in the strong and weak interaction limits it is convenient to group them into five sets of four transitions each. To first order the fields at which the transitions occur at constant frequency and the corresponding transition probabilities are given in eq 8–12 in which $g = (g_1 + g_2)/2$, $H_0 = h\nu/(g\beta)$, and $H_M = h\nu/(g_1\beta)$.

group 1: transitions 2 → 1 (a), 3 → 1 (b), 12 → 10 (c), and 12 → 11 (d)

$$H_{a,b} = H_o + \frac{1}{g\beta}[-\tfrac{1}{2}(A_1m_1 + A_2m_2) - 1.5J \pm \mathrm{EF2}(5/2)] \quad (8)$$

$$\mathrm{PROB_a} = (-B(5/2) + C(5/2)\sqrt{5})^2$$

$$\mathrm{PROB_b} = (C(5/2) + B(5/2)\sqrt{5})^2$$

$$H_{c,d} = H_o + \frac{1}{g\beta}[-\tfrac{1}{2}(A_1m_1 + A_2m_2) + 1.5J \mp \mathrm{EF2}(-3/2)]$$

$$\mathrm{PROB_c} = (C(-3/2) - B(-3/2)\sqrt{5})^2$$

$$\mathrm{PROB_d} = (B(-3/2) + C(-3/2)\sqrt{5})^2$$

group 2: transitions 4 → 3, 6 → 5, 8 → 7, and 10 → 9

$$H = H_M + \frac{1}{g\beta}[-A_1m_1 + \mathrm{EF2}(M_1) + \mathrm{EF2}(M_1 - 1)] \quad (9)$$

$$M_1 = 5/2, 3/2, 1/2, -1/2$$

$$\mathrm{PROB} = (-C(M_1)B(M_1 - 1)(8.75 - M_1(M_1 - 1))^{1/2} - B(M_1)B(M_1 - 1) + B(M_1)(C(M_1 - 1)(8.75 - (M_1 - 1)(M_1 - 2))^{1/2})^2$$

group 3: transitions 5 → 3, 7 → 5, 9 → 7, and 11 → 9

(16) Eaton, S. S.; More, K. M.; DuBois, D. L.; Boymel, P. M.; Eaton, G. R. *J. Magn. Reson.* **1980**, *41*, 150–157.
(17) More, K. M.; Eaton, G. R.; Eaton, S. S. *Inorg. Chem.* **1984**, *23*, 1165–1170.
(18) Charles, R. G. *Inorg. Synth.* **1960**, *6*, 164–166.
(19) Gurevich, M. Z.; Sas, T. M.; Zelentsov, V. V.; Stepin, B. D.; Mazepova, N. E.; *Russ. J. Inorg. Chem. (Engl. Transl.)* **1975**, *20*, 250–254.
(20) Morris, M. L.; Moshier, R. W.; Sievers, R. E. *Inorg. Chem.* **1963**, *2*, 411–412.
(21) Pirrwitz, J.; Damerau, W. *Z. Chem.* **1976**, *16*, 401–402.

$$H = H_M + \frac{1}{g\beta}[-A_1 m_1 + EF2(M_1) - EF2(M_1 - 1)] \quad (10)$$

$$M_1 = 5/2, 3/2, 1/2, -1/2$$

$$PROB = (C(M_1)C(M_1 - 1)(8.75 - M_1(M_1 - 1))^{1/2} + B(M_1)C(M_1 - 1) + B(M_1)B(M_1 - 1)(8.75 - (M_1 - 1)(M_1 - 2))^{1/2})^2$$

group 4: transitions $4 \rightarrow 2$, $6 \rightarrow 4$, $8 \rightarrow 6$, and $10 \rightarrow 8$

$$H = H_M + \frac{1}{g\beta}[-A_1 m_1 - EF2(M_1) + EF2(M_1 - 1)] \quad (11)$$

$$PROB = (B(M_1)B(M_1 - 1)(8.75 - M_1(M_1 - 1))^{1/2} - C(M_1)B(M_1 - 1) + C(M_1)C(M_1 - 1)(8.75 - (M_1 - 1)(M_1 - 2))^{1/2})^2$$

group 5: transitions $5 \rightarrow 2$, $7 \rightarrow 4$, $9 \rightarrow 6$, and $11 \rightarrow 8$

$$H = H_M + \frac{1}{g\beta}[-A_1 m_1 - EF2(M_1) - EF2(M_1 - 1)] \quad (12)$$

$$M_1 = 5/2, 3/2, 1/2, -1/2$$

$$PROB = (-B(M_1)C(M_1 - 1)(8.75 - M_1(M_1 - 1))^{1/2} + C(M_1)C(M_1 - 1) + B(M_1 - 1)C(M_1)(8.75 - (M_1 - 1)(M_1 - 2))^{1/2})^2$$

The second-order corrections to the energy levels due to the terms in eq 3 are given in Table I. These were used to calculate the second-order corrections to the resonant fields. The assignments of the transitions in the limits of strong and weak interaction are given in Table II. These assignments were used in choosing the line widths for the transitions. Three approaches were used to determine line widths. Method I: The line width for each transition was a linear combination of the metal and nitroxyl line widths (WM and WN, respectively) with the weightings determined by the coefficients of the metal and nitroxyl contributions to the transition probability. Method 2: The line width for each transition was determined by whether it was an $S = 2$ or $S = 3$ transition in the limit of strong exchange. Method 3: The line width for each transition was based on whether it was a nitroxyl line, metal inner line, or metal outer line in the limit of weak exchange. For each of the methods the line width was assumed to be dependent on the manganese electron spin state and independent of the manganese nuclear spin state. For each of the simulated spectra one of the line width methods gave better results than the others as discussed below.

In the weak exchange limit, for each combination of a manganese nuclear spin state and a nitroxyl nitrogen nuclear spin state, each of the five manganese lines ($S = -5/2 \rightarrow -3/2, -3/2 \rightarrow -1/2, -1/2 \rightarrow 1/2, 1/2 \rightarrow 3/2, 3/2 \rightarrow 5/2$) is split into a doublet, and each nitroxyl line is split into six equally intense, equally spaced lines. This is the expected first-order pattern. Inclusion of the manganese nuclear spin ($I = 5/2$) and the nitroxyl nitrogen nuclear spin ($I = 1$) gives 6×3 such subspectra and a total of 288 lines. In this limit the manganese and nitroxyl nuclear hyperfine splittings are the same as observed in the absence of spin–spin interaction. The relative intensities of the manganese and nitroxyl lines are those expected from the respective transition probability expressions for independent spins (total Mn intensity/total nitroxyl intensity = 11.67).

The validity of the equations for the transition energies and probabilities was tested by comparison with prior results obtained for limiting cases. If the nuclear hyperfine terms are deleted from eq 4–12 the equations reduce to those reported by Corio for the $I_A = 5/2$ component of an A_5B $I = 1/2$ pattern.[22]

When J is large relative to the energy separation between the manganese and nitroxyl lines (strong exchange) the calculated spectrum is a superposition of $S = 2$ (four transitions) and $S = 3$ (six transitions) contributions. Transitions between the two spin states have negligible intensity and are designated as forbidden in Table II. The wave functions in this limit agree with those reported previously for a Cu(II)–Mn(II) dimer with strong exchange interaction.[23] The manganese and nitroxyl nuclear hyperfine splittings in the $S = 2$ state are $7/6$ and $1/6$, respectively, of the corresponding values in the absence of exchange. In the $S = 3$ state the ratios are $5/6$ and $1/6$, respectively. These ratios agree with those calculated from the equations obtained by other authors for the strong exchange limit.[23-25]

The correlation between the transitions in the weak and strong exchange limits is as follows. Within each weak exchange nitroxyl sextet, the line which is originally the closest to the manganese lines moves toward the manganese lines as J increases and becomes one of the strong exchange $S = 3$ transitions. The other five nitroxyl lines move away from the manganese lines, rapidly losing intensity, and become forbidden transitions. From each of the five manganese doublets the component closer to the nitroxyl lines (subsequently called a manganese inner line) moves toward the nitroxyl lines, and these become five of the six components of the $S = 3$ manifold. The components of the five manganese doublets which are further away from the nitroxyl lines are referred to as manganese outer lines. The manganese outer line which is furthest from the nitroxyl lines moves rapidly away from the nitroxyl lines as J increases, loses intensity, and becomes a forbidden line. The other four manganese outer lines move away from the nitroxyl lines and become the $S = 2$ transitions. Due to the small g value difference between the nitroxyl and manganese electrons and the relatively small value of A_{Mn}, a value of J of about 200×10^{-4} cm^{-1} is large enough to achieve the strong exchange limit.

Results and Discussion

Solution Equilibria. In dichloromethane solution the X-band EPR spectrum of $Mn(tfac)_2$ is broad with a peak-to-peak width of about 500 G. The manganese nuclear hyperfine splitting is not resolved. Addition of pyridine to the solution results in the appearance of sharper signals with peak-to-peak line widths of 32 G and $A_{Mn} = 92$ G. This spectrum was assigned to $Mn(tfac)_2py$. Quantitation of the sharp signal as a function of the concentration of pyridine added gave a pyridine binding constant of 3×10^2 M at room temperature. When spin-labeled bidentate ligand III was added to dichloromethane solutions of $Mn(tfac)_2$ the intensity of the signal for the ligand that was not coordinated indicated a binding constant of 5×10^3 M. When $Mn(tfac)_2$ was added to solutions of 2,2,6,6-tetramethylpiperidinyl-1-oxy in dichloromethane there was a decrease in the integrated intensity of the nitroxyl EPR signal. The loss of signal indicates that when a nitroxyl oxygen coordinates to Mn(II) there is strong spin–spin interaction, and the resulting complex does not give an observable EPR signal under the conditions used to observe the normal room temperature EPR spectrum of a nitroxyl radical. A similar loss of the nitroxyl EPR signal upon coordination of the nitroxyl oxygen to Cu(II) and VO(IV) has been observed.[26] The loss of the nitroxyl signal as a function of the concentration of $Mn(tfac)_2$ in toluene solution indicated a binding constant of about 100 M. This value is in reasonable agreement with values obtained for coordination of nitroxyl oxygen to $Cu(tfac)_2$ ($K = \sim 25$ M in CCl_4) and to $VO(tfac)_2$ ($K = 400$ M in dichloromethane).[26] Thus the binding of a nitroxyl oxygen to Mn(II) is slightly less favorable than the binding of pyridine and substantially less favorable than the binding of bidentate nitrogenous bases.

Since the EPR spectrum of $Mn(tfac)_2$ in fluid solution is much broader than the spectrum of $Mn(tfac)_2py$, excess $Mn(tfac)_2$ does not interfere with observations of the spectrum of the pyridine adduct. Therefore the spectra of the $Mn(tfac)_2$ adducts of

(22) Corio, P. L. "Structures of High-Resolution NMR Spectra"; Academic Press: New York, 1966; pp 208–216.

(23) Paulson, J. A.; Krost, D. A.; McPherson, G. L.; Rogers, R. D.; Atwood, J. L. *Inorg. Chem.* **1980**, *19*, 2519–2525.

(24) Banci, L.; Bencini, A.; Dei, A.; Gatteschi, D. *Inorg. Chem.* **1981**, *20*, 393–398.

(25) Chao, C.-C. *J. Magn. Reson.* **1973**, *10*, 1–6.

(26) Sawant, B. M.; Eaton, G. R.; Eaton, S. S. *J. Magn. Reson.* **1981**, *45*, 162–169 and references therein.

Table I. Second-Order Corrections to the Energy Levels[a]

E_1: $(A_1^2/4\omega_o)[5(8.75 - m_1(m_1 + 1))]$

E_2: $(A_1^2/4\omega_0)[[(B(^3/_2)B(^5/_2)\sqrt{5} + C(^3/_2)C(^5/_2)2\sqrt{2})^2 + (-C(^3/_2)B(^5/_2)\sqrt{5} + B(^3/_2)C(^5/_2)2\sqrt{2})^2](8.75 - m_1(m_1 + 1)) - 5C(^5/_2)^2(8.75 - m_1(m_1 - 1))]$

E_3: $(A_1^2/4\omega_0)[[(-B(^3/_2)C(^5/_2)\sqrt{5} + C(^3/_2)B(^5/_2)2\sqrt{2})^2 + (C(^3/_2)C(^5/_2)\sqrt{5} + B(^3/_2)B(^5/_2)2\sqrt{2})^2](8.75 - m_1(m_1 + 1)) - 5B(^5/_2)^2(8.75 - m_1(m_1 - 1))]$

E_4: $(A_1^2/4\omega_0)[[(B(^1/_2)B(^3/_2)2\sqrt{2} + C(^1/_2)C(^3/_2)3)^2 + (-C(^1/_2)B(^3/_2)2\sqrt{2} + B(^1/_2)C(^3/_2)3)^2](8.75 - m_1(m_1 + 1)) - [(B(^3/_2)B(^5/_2)\sqrt{5} + C(^3/_2)C(^5/_2)2\sqrt{2})^2 + (-B(^3/_2)C(^5/_2)\sqrt{5} + C(^3/_2)B(^5/_2)2\sqrt{2})^2](8.75 - m_1(m_1 - 1))]$

E_5: $(A_1^2/4\omega_o)[[(-B(^1/_2)C(^3/_2)2\sqrt{2} + C(^1/_2)B(^3/_2)3)^2 + (C(^1/_2)C(^3/_2)2\sqrt{2} + B(^1/_2)B(^3/_2)3)^2](8.75 - m_1(m_1 + 1)) - [(-C(^3/_2)B(^5/_2)\sqrt{5} + B(^3/_2)C(^5/_2)2\sqrt{2})^2 + (C(^3/_2)C(^5/_2)\sqrt{5} + B(^3/_2)B(^5/_2)2\sqrt{2})^2](8.75 - n_1(m_1 - 1))]$

E_6: $(A_1^2/4\omega_o)[[(B(^{-1}/_2)B(^1/_2)3 + C(^{-1}/_2)C(^1/_2)2\sqrt{2})^2 + (-C(^{-1}/_2)B(^1/_2)3 + B(^{-1}/_2)C(^1/_2)2\sqrt{2})^2](8.75 - m_1(m_1 + 1)) - [(B(^1/_2)B(^3/_2)2\sqrt{2} + C(^1/_2)C(^3/_2)3)^2 + (-B(^1/_2)C(^3/_2)2\sqrt{2} + C(^1/_2)B(^3/_2)3)^2](8.75 - m_1(m_1 - 1))]$

E_7: $(A_1^2/4\omega_o)[[(-B(^{-1}/_2)C(^1/_2)3 + C(^{-1}/_2)B(^1/_2)2\sqrt{2})^2 + (C(^{-1}/_2)C(^1/_2)3 + B(^{-1}/_2)B(^1/_2)2\sqrt{2})^2](8.75 - m_1(m_1 + 1)) - [(-C(^1/_2)B(^3/_2)2\sqrt{2} + B(^1/_2)C(^3/_2)3)^2 + (C(^1/_2)C(^3/_2)2\sqrt{2} + B(^1/_2)B(^3/_2)3)^2](8.75 - m_1(m_1 - 1))]$

E_8: $(A_1^2/4\omega_o)[[B(^{-3}/_2)B(^{-1}/_2)2\sqrt{2} + C(^{-3}/_2)C(^{-1}/_2)\sqrt{5})^2 + (-C(^{-3}/_2)B(^{-1}/_2)2\sqrt{2} + B(^{-3}/_2)C(^{-1}/_2)\sqrt{5})^2](8.75 - m_1(m_1 + 1)) - [(B(^{-1}/_2)B(^1/_2)3 + C(^{-1}/_2)C(^1/_2)2\sqrt{2})^2 + (-B(^{-1}/_2)C(^1/_2)3 + C(^{-1}/_2)B(^1/_2)2\sqrt{2})^2](8.75 - m_1(m_1 - 1))]$

E_9: $(A_1^2/4\omega_o)[[-B(^{-3}/_2)C(^{-1}/2)2\sqrt{2} + C(^{-3}/_2)B(^{-1}/_2)\sqrt{5})^2 + (C(^{-3}/_2)C(^{-1}/_2)2\sqrt{2} + B(^{-3}/_2)B(^{-1}/_2)\sqrt{5})^2](8.75 - m_1(m_1 + 1)) - [(-C(^{-1}/_2)B(^1/_2)3 + B(^{-1}/_2)C(^1/_2)2\sqrt{2})^2 + (C(^{-1}/_2)C(^1/_2)3 + B(^{-1}/_2)B(^1/_2)2\sqrt{2})^2](8.75 - m_1(m_1 - 1))]$

E_{10}: $(A_1^2/4\omega_o)[5(B(^{-3}/_2)^2(8.75 - m_1(m_1 + 1)) - [(B(^{-3}/_2)B(^{-1}/_2)2\sqrt{2} + C(^{-3}/_2)C(^{-1}/_2)\sqrt{5})^2 + (-B(^{-3}/_2)C(^{-1}/_2)2\sqrt{2} + C(^{-3}/_2)B(^{-1}/_2)\sqrt{5})^2](8.75 - m_1(m_1 - 1))]$

E_{11}: $(A_1^2/4\omega_o)[5(C(^{-3}/_2)^2(8.75 - m_1(m_1 + 1)) - [(-C(^{-3}/_2)B(^{-1}/_2)2\sqrt{2} + B(^{-3}/_2)C(^{-1}/_2)\sqrt{5})^2 + (C(^{-3}/_2)C(^{-1}/_2)2\sqrt{2} + B(^{-3}/_2)B(^{-1}/_2)\sqrt{5})^2](8.75 - m_1(m_1 - 1))]$

E_{12}: $(A_1^2/4\omega_o)[5(8.75 - m_1(m_1 - 1))]$

[a] $\omega_o = h\nu$, coefficients B and C are defined in eq 6 and 7.

Table II. Assignments of Transitions[a]

group	$\delta^b < 0$		$\delta^b > 0$	
	small J	large J	small J	large J
1a	nitroxyl	$S = 3$	Mn	$S = 3$
1b	Mn	forbidden	nitroxyl	forbidden
1c	Mn	$S = 3$	nitroxyl	$S = 3$
1d	nitroxyl	forbidden	Mn	forbidden
2	nitroxyl	forbidden	forbidden	forbidden
3	Mn	$S = 2$	Mn	$S = 2$
4	Mn	$S = 3$	Mn	$S = 3$
5	forbidden	forbidden	nitroxyl	forbidden

[a] See text for discussion of the transitions. [b] $\delta = \beta H(g_1 - g_2) + (A_1m_1 - A_2m_2)$.

monodentate ligands I, II, IV, V, and VIII to XI were obtained in the presence of excess $Mn(tfac)_2$ to minimize the interference from the sharp nitroxyl signal of ligand that was not coordinated. The line widths of the manganese lines in the six-coordinate $Mn(tfac)_2$ adducts of bidentate ligands III, VI, VII, and XII were broader than the line widths for the five-coordinate adducts and similar to the line widths for $Mn(tfac)_2$. However, the binding constants for the bidentate ligands were larger than for the monodentate ligands so there was little interference from the signals from either free ligand or $Mn(tfac)_2$ in the equimolar mixtures which were used to obtain the EPR spectra.

Analysis of the equilibria involving $Mn(hfac)_2$ was more difficult than for $Mn(tfac)_2$ due to the low solubility of $Mn(hfac)_2$ in the absence of coordinating solvents. The most convenient method for preparation of solutions of $Mn(hfac)_2$ was to dissolve the $Mn(hfac)_2$ in a minimum volume of acetone and dilute to the desired concentration with toluene or CH_2Cl_2. Solutions prepared in this manner gave a well-resolved X-band EPR spectrum with a peak-to-peak width of about 65 G and A_{Mn} of about 92 G which was assumed to be the spectrum of the acetone adduct. The acetone was readily displaced by nitrogenous bases but competed effectively with the nitroxyl oxygen. Although the competitive equilibria were not analyzed quantitatively, it was evident that for the monodentate spin-labeled pyridine derivatives the ratio of pyridine nitrogen coordination to nitroxyl oxygen coordination was higher for $Mn(hfac)_2$ in the presence of acetone than for $Mn(tfac)_2$. In equimolar mixtures of spin-labeled ligand and $Mn(hfac)_2$ in toluene/acetone the dominant species was the spin-labeled adduct and there was minimal interferences from other species.

Comparison of X-band and Q-band EPR Spectra. The peak-to-peak line widths in the EPR spectrum of $Mn(tfac)_2py$ in dichloromethane solution were 43 G at X-band and 24 G at Q-band. For $Mn(hfac)_2py$ the line widths were too broad to allow resolution of the nuclear hyperfine splitting at X-band and decreased to 40 G at Q-band. Quantitation of the X-band spectra indicated that all five of the manganese transitions contributed to the observed spectrum although simulations indicated that the line widths for the $-^1/_2 \rightarrow +^1/_2$ transition were substantially smaller than the line widths for the other transitions. At Q-band only the $-^1/_2 \rightarrow +^1/_2$ transitions were observed. Similar changes between X-band and Q-band spectra of Mn(II) have been discussed previously.[27] There is no first-order contribution of the Mn(II) zero field splitting (ZFS) to the energy of the $-^1/_2 \rightarrow +^1/_2$ transition. Since the ZFS terms are the dominant contributions to the anisotropy of the spectra of Mn(II), even moderate tumbling rates are sufficient to cause motional averaging of the $-^1/_2 \rightarrow +^1/_2$ transition, and the line widths for this transition are relatively small. Since the only contributions of the ZFS to the anisotropy of this transition are from second-order or higher terms, these contributions are inversely dependent on spectrometer frequency, and the lines are sharper at higher frequency. For the four other manganese transitions the ZFS contributes to the transition energy to first order. Thus, faster tumbling rates are required to provide motional averaging of the anisotropies of these transitions than for the $-^1/_2 \rightarrow +^1/_2$ transition, and the anisotropies do not decrease as the spectrometer frequency increases.

It has also been noted that metal relaxation rates decrease as frequency increases which would also cause narrower lines at Q-band than at X-band.[27,28] The relative importance of the two factors is not known. In the complexes examined here the line widths are greater both at X-band and at Q-band for the adducts of the larger $Mn(hfac)_2$ than for adducts of the smaller $Mn(tfac)_2$. This dependence on molecular size suggests that incomplete motional averaging may be an important factor in the line widths and that the changes in line width between X-band and Q-band may be dominated by incomplete motional averaging of the ZFS.

Effect of Electron–Electron Spin–Spin Interaction on the EPR Spectra. When spin-labeled ligand VII coordinated to $Mn(hfac)_2$ the nitroxyl lines in the X-band spectrum were broad, and the manganese lines were poorly resolved. Simulation of the spectra indicated an electron–electron coupling constant, J, less than 1×10^{-4} cm^{-1} and a nitroxyl line width of about 10 G. In this complex there was significant broadening of the nitroxyl lines and a weak spin–spin interaction.

Figure 1 shows the changes in the X-band EPR spectra as the value of J increases. The nitroxyl lines spread apart and approach the extent of the manganese spectrum. The poor resolution of the nitroxyl lines was due both to the broadening of the lines and to the large number of transitions which occur as a result of interaction with manganese. In a 1:1 mixture of $Mn(hfac)_2$ and

(27) Reed, G. H.; Ray, W. J., Jr. *Biochemistry* **1971**, *10*, 3190–3197.
(28) Rubenstein, M.; Baram, A.; Luz, Z. *Mol. Phys.* **1971**, *20*, 67–80.

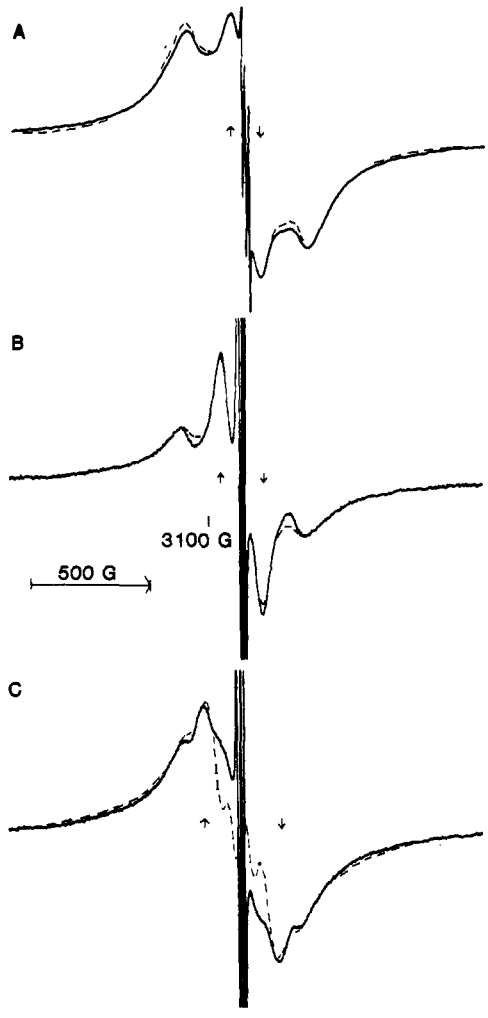

Figure 1. X-band (9.105 GHz) EPR spectra (2000-G scans) at room temperature. (A) $Mn(hfac)_2$·XII in toluene/acetone solution. The spectrum was obtained with 40-mW power and 2.5-G modulation amplitude. (B) $Mn(hfac)_2$·VIII in CH_2Cl_2/acetone solution. The spectrum was obtained with 20-mW power and 2.5-G modulation amplitude. (C) $Mn(hfac)_2$·XI in CH_2Cl_2/acetone solution. The spectrum was obtained with 20-mW power and 3.2-G modulation amplitude. The dashed lines denote the simulated spectra in regions where the simulations do not coincide with the experimental curves. The values of J used in the simulations of the spectra in parts A, B, and C are 14×10^{-4}, 32×10^{-4}, and 62×10^{-4} cm^{-1}, respectively. The values of other parameters used in the simulations are given in Table III.

ligand XII most of the ligand was coordinated, so the sharp three-line nitroxyl signal characteristic of ligand that was not coordinated was small (Figure 1A). The signal for the coordinated ligand was severely broadened and was simulated by assuming an electron–electron coupling constant of 14×10^{-4} cm^{-1} (Table III). The manganese lines were broad as was observed for all of the six-coordinate complexes examined. The line widths in this spectrum could be simulated by using either line-width method 1 or 3 discussed above although method 1 appeared to be preferable. The arrows in the figure indicate the low-field and high-field extrema for the nitroxyl transitions. (Throughout the text transitions are denoted by the nature of the transition in the limit of strong or weak exchange.) Monodentate ligand VIII did not bind as strongly to $Mn(hfac)_2$ as the bidentate ligands, so there was a larger signal for ligand that was not coordinated to Mn(II) in Figure 1B than in Figure 1A. However, most of the nitroxyl intensity was in the broad signal that falls between the two arrows. The simulation of the nitroxyl signal required a value of J of 30×10^{-4} cm^{-1}. The manganese lines were poorly resolved. The broad wings of the spectrum indicated that the line widths for some of the manganese transitions were much broader than for the $-1/2 \rightarrow 1/2$ transition. When line width method 1 was used

Table III. Parameters Used in the Simulations of the Spectra Shown in Figures 1–3[a]

figure	J, 10^{-4} cm^{-1}	A_{Mn} 10^{-4} cm^{-1}	line-width method[b]	line widths,[c,d] G
1A	14	85.5	1	WN = 60 WM = 300, 200, 110, 200, 300
1b	30	85.5	3	WN = 45 WMO = 1200, 800, 120, 800, 1200 WMI = WMO
1C	62	86.5	3	WN = 55 WMO = 800, 700, 600, 700, 800 WMI = 500, 400, 110, 400, 500
2A	6	85.5	1	WN = 20 WM = 200, 100, 35, 100, 200
2B	112	87.0	3	WN = 38 WMO = 1200, 800, 200, 800, 1200 WMI = 1200, 600, 65, 600, 1200
3A	200	86.0	2	W2 = 400, 300, 300, 400 W3 = 240, 200, 150, 150, 200, 240
3B	200	86.0	2	W2 = 800, 300, 300, 800 W3 = 800, 600, 87, 87, 600, 800

[a] The following parameters were used in all of the simulations: Mn, $g = 2.004$; nitroxyl, $g = 2.0056$; $A_N = 14.5–15.5 \times 10^{-4}$ cm^{-1}, depending on the size of the nitroxyl ring. [b] Definitions of the line-width methods are given in the text. [c] The line widths were assumed to be dependent on the manganese electron spin state and independent of the manganese nuclear spin state. WN = line width for nitroxyl contribution to a transition (method 1) or line width for a transition which is a nitroxyl transition in the limit of small J (method 3). WM = line width for metal contribution to a transition. WMO, WMI = line widths for outer and inner components, respectively, of the manganese doublets. W2, W3 = line widths for the $S = 2$ and $S = 3$ transitions, respectively, in the limit of large J. [d] Although the line widths for the sharpest manganese lines are accurate to ±5 G, the line widths for the other manganese transitions are only approximate.

in the simulation of this spectrum, the large line widths of some of the manganese lines and the extensive mixing of the manganese and nitroxyl contributions to the transitions resulted in excessive broadening of the nitroxyl lines. It appears that the factors which contribute to the broadening of the manganese lines do not contribute to the broadening of the spin-coupled transitions proportional to the coefficients in the transition probability expressions. Improved simulations were obtained with line-width method 3, although this did not give exact match with the wings of the spectra. The spectra of $Mn(hfac)_2$·XI (Figure 1C) show that the nitroxyl intensity has spread out further in this complex than in the complexes of ligands VIII and XII consistent with an increase in the value of J. Simulation of the spectra required a value of J of 62×10^{-4} cm^{-1} and the use of line-width method 3. As in the X-band spectra of the other complexes, the manganese lines were poorly resolved and provided little information concerning the spin–spin interaction.

At Q-band the manganese lines were significantly narrower than at X-band that in some cases it was possible to obtain information concerning the value of J from the manganese lines as well as the nitroxyl lines. The values of J obtained from the Q-band spectra were consistent with the values obtained from the X-band spectra. Figure 2A shows the Q-band spectrum of $Mn(tfac)_2$·I. The three sharp nitroxyl lines dominated the center of the spectrum. Five of the six manganese lines (due to the manganese nuclear spin) were observable with line widths of about 35 G. Simulation of the spectrum indicated that the value of J must be $<10 \times 10^{-4}$ cm^{-1}. Larger values caused significant distortion of the manganese lines. The value of J for this complex was sufficiently small that either line width method 1 or 3 provided adequate results. The Q-band spectrum of $Mn(tfac)_2$·IV is shown in Figure 2B. The sharp three line nitroxyl spectrum in Figure 2B was much less intense than in Figure 2A because the sharp signal in Figure 2B was due only to ligand which was not coordinated whereas the sharp signal in Figure 2A was due to coordinated ligand as well as ligand which was not coordinated. The simulation of the spectrum in Figure 2B was obtained with $J = 112 \times 10^{-4}$ cm^{-1}. Satisfactory simulation of the spectrum could only be obtained

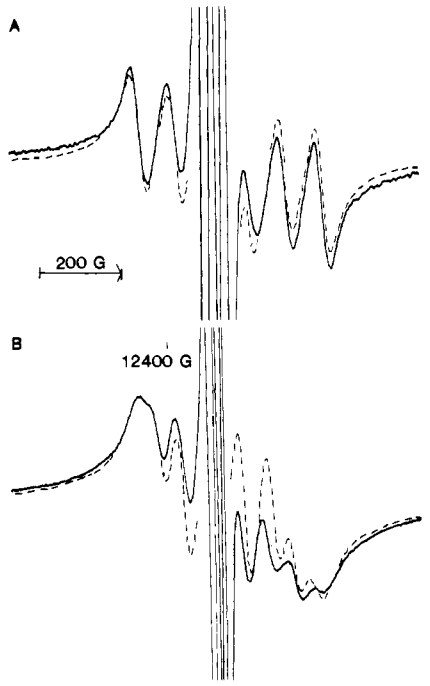

Figure 2. Q-band (35.25 GHz) EPR spectra (1000-G scans) at room temperature. (A) $Mn(tfac)_2$·I in CH_2Cl_2 solution. The spectrum was obtained with 148-mW power and 1.25-G modulation amplitude. (B) $Mn(tfac)_2$·IV in CH_2Cl_2 solution. The spectrum was obtained with 148-mW power and 2.5-G modulation amplitude. The dashed lines denote the simulated spectra in regions where the simulations do not coincide with the experimental curves. The values of J used in the simulations of the spectra in parts A and B are 6×10^{-4} and 112×10^{-4} cm^{-1}, respectively. The values of other parameters used in the simulations are given in Table III.

with line-width method 3. It is evident from the discrepancy between the observed and calculated spectra that the experimental line widths are dependent on the manganese nuclear spin state although this dependence was not included in the simulation. With a J value of this magnitude, the nitroxyl and manganese lines were almost fully averaged except for the lines with manganese $m_I = \pm 5/2$. Thus, the splittings of the lowest and highest field peaks were the features of the simulated spectrum which were most sensitive to changes in the value of J. The manganese outer lines ($S = 2$) were substantially broader than the manganese inner lines ($S = 3$) that dominated the spectrum. The use of line-width method 3 was necessary to permit different line widths for the various $S = 3$ transitions dependent on whether the transition was a manganese line or a nitroxyl line in the limit of weak interaction.

Although the spectrum in Figure 2B is approaching the strong exchange limit, the changes in the resonant fields for the major peaks on going from the spectrum in Figure 2A to the one in Figure 2B are relatively small. The small change is the net result of several factors. (1) The manganese and nitroxyl g values are close together, and therefore there is little change in the center of the manganese spectrum on going from weak to strong exchange. (2) The manganese lines are so much more intense than the nitroxyl lines that the appearance of the spectra is dominated by the manganese lines except when the nitroxyl lines are much sharper than the manganese lines. (3) The manganese hyperfine splitting of the strong exchange $S = 3$ lines is $5/6$ of the value in the absence of spin–spin interaction. This small change in the hyperfine splitting is the major distinction between the weak and strong exchange spectra. Thus, it could be quite easy to mistake a strong exchange spectrum for that of a weakly interacting spin system. This problem is particularly serious at X-band where the hyperfine splitting is not well resolved and an increase in line width could mask the decrease in the hyperfine splitting.

The spectra in Figure 3 are strong exchange spectra of $Mn(tfac)_2$·VI obtained at X-band and Q-band. In both cases the lines for the $S = 2$ components were substantially broader than for the

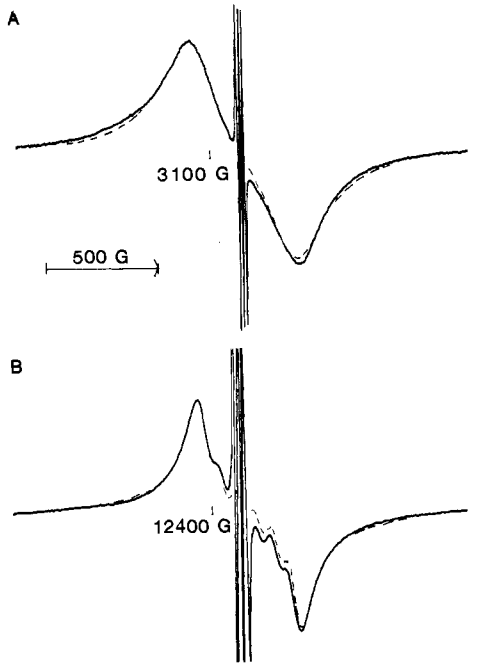

Figure 3. EPR spectra (2000-G scans) of $Mn(tfac)_2$·VI in CH_2Cl_2 solution. (A) X-band spectrum obtained with 5-mW power and 4-G modulation amplitude. (B) Q-band spectrum obtained with 47-mW power and 2-G modulation amplitude. The dashed lines denote the simulated spectra in regions where the simulations do not coincide with the experimental curves. The value of J for the simulations was 200×10^{-4} cm^{-1}. The values of other parameters used in the simulations are given in Table III.

Table IV. Values of J^a for $Mn(tfac)_2$·L and $Mn(hfac)_2$·L and Comparison with Values of J for Related Cu(II)[c,d] and VO(IV)[d,e] Adducts

ligand	J_{Mn}[b]	J_{VO}[c,d]	J_{Cu}[d,e]
I	≤10	110 (2)	43 (14)
II	≤10	32 (2)	63 (14)
III	≥200	*f*	>1000 (14)
IV	112	1750 (2)	600 (15)
V	≤10	400 (2)	475 (15)
VI	≥200	*f*	>2000 (15)
VII	≤1[g]	*f*	30
VIII	30	420 (2)	155 (2)
IX	≤10	87 (2)	58 (2)
X	32	380 (2)	155 (2)
XI	62	490 (3)	220 (3)
XII	14[g]	*f*	300

[a] In units of 10^{-4} cm^{-1}. The sign of J is not known. [b] In fluid solution at room temperature. Values of J were the same within experimental error for the $Mn(tfac)_2$ and $Mn(hfac)_2$ adducts. Spectra were analyzed at X-band and Q-band unless otherwise noted. [c] Average of values for $VO(tfac)_2$·L and $VO(hfac)_2$·L. [d] The number of the reference from which the data were taken is indicated in parentheses. [e] Values for $Cu(hfac)_2$·L. [f] The bidentate ligands do not bind well to $VO(tfac)_2$ or $VO(hfac)_2$. [g] Based on X-band spectra.

$S = 3$ components which dominated the spectra. The simulated spectra indicated that the manganese and nitroxyl lines were fully averaged by the spin–spin interaction. Line-width method 2 was used in the simulations of the spectra. Although the lines in the Q-band spectrum were substantially narrower than in the X-band spectrum, the difference between X-band and Q-band was much smaller for these six-coordinate complexes than was observed (Figures 1 and 2) for the five-coordinate complexes. Also at both X-band and Q-band the manganese line widths in the six-coordinate complexes were consistently larger than for the five-coordinate complexes. These observations suggest that the ZFS is larger for the six-coordinate complexes than for the five-coordinate complexes.

Comparison with Copper and Vanadyl Complexes of the Same Ligands. The value of J for the Mn(II) complexes of 4-substituted

ligand IV is about an order of magnitude larger than for the analogous complexes of 3-substituted ligand V (Table IV). Similarly the value of J for the complexes of 4-substituted ligand VIII is at least a factor of 3 larger than for the analogous complexes of 3-substituted ligand IX. The observation of substantially larger spin–spin interaction at the 4-position of the pyridine ring than at the 3-position parallels previous observations for vanadyl complexes of the same types of ligands (table IV) in which the pyridine π orbitals play a major role in the spin delocalization.[2] In the copper complexes σ interaction was important, and the values of J were similar for 4- and 3-substituted ligands.[2] Thus, π delocalization appears to be important in the Mn(II) complexes. The value of J for the complexes of ligand VIII which has an amide linkage at the 4-position of the pyridine ring is smaller than the value of J for the complexes of ligand X which has a urea linkage at the pyridine 4-position. The larger value of J for a urea linkage than for an amide linkage has previously been observed in systems where π delocalization of the unpaired spin density is significant.[3,29] This observation lends further support to the proposal that π delocalization is important in these manganese systems. The similarity in the values of J for the complexes of VIII and X which contain unsaturated five- and six-membered nitroxyl rings, respectively, is consistent with previous results obtained for these ligands with other metals.[2,30,31] The size of the unsaturated nitroxyl ring appears to have little impact on the magnitude of J when there is significant π delocalization. Thus, the observed pattern of spin delocalization indicates that although Mn(II) has unpaired electrons in d orbitals which have the requisite symmetry for either σ or π interaction with the pyridine oribitals, π interaction dominates. It must be noted, however, that both σ and π delocalization are probably present and that the value of J is a monitor of the net spin delocalization through the entire metal–nitroxyl linkage.

The observation of strong exchange for the complexes of the 2-substituted ligands III and VI is consistent with results obtained previously for the analogous copper complexes.[14,15] The coordination of the azine nitrogen to the metal provides a relatively short pathway for interaction and results in strong exchange. Richardson and Kreilick observed strong exchange between Mn(II) and coordinated 2-pyridyliminonitroxyl and 2-pyridyl nitonyl nitroxide. In these complexes, also, there is a short bond pathway between the metal and the nitroxyl.[32] The value of J was about -105 cm^{-1}, and the ground state was $S = 2$. The observed EPR signal was that of the $S = 3$ excited state which is consistent with our observation that the line widths for the $S = 2$ transitions are larger than for $S = 3$.

When 2-substituted ligand VII is coordinated to Mn(II) the spin–spin interaction caused only a broadening of the nitroxyl lines. Thus, the longer metal–nitroxyl linkage and the presence of the two CH_2 groups in the Mn(II)–nitroxyl linkage cause a large decrease in the value of J. Even though ligand XII has a saturated carbon between the coordinated nitrogen and the amide linkage to the nitroxyl ring, a value of J of 14×10^{-4} cm^{-1} was observed for the manganese complex. Thus, some spin delocalization can occur through σ linkages even though the preferred pathway appears to be π interaction.

Since π effects appear to dominate the spin delocalization for the manganese ($S = {}^5/_2$) and vanadyl ($S = {}^1/_2$) complexes, comparison of the values of J for these two metals should indicate the effect of the metal spin on the spin–spin coupling. The values of J for the Mn(II) complexes are about an order of magnitude smaller than for the vanadyl complexes of the same ligands. A decrease in J by a factor of 5 would be expected on going from an $S = {}^1/_2$ to an $S = {}^5/_2$ metal for an interaction through a single pair of orbitals.[33] For Mn(II) there is the possibility of interaction of each of the metal unpaired electrons with the nitroxyl unpaired electron. It is likely that some of these interactions make positive contributions to J and others make negative contributions. The decrease in J by more than a factor of five may be due to partial cancellation of contributions with different signs. Although small structural differences may also contribute to changes in the value of J it is unlikely that the large differences observed here are solely structural. A comparison of Cu(II) and Co(II) complexes in which σ delocalization was dominant indicated substantial similarities in the values of J for the two metals.[30,31] It seems more likely that the dramatic decrease in the value of J on going from $S = {}^1/_2$ to $S = {}^5/_2$ is due to the change in the electronic structure of the metal. This result is in good agreement with the earlier proposal that changes in the value of J in homonuclear and heteronuclear metal dimers reflected the changes in the number of unpaired electrons on the metal and were not due entirely to structural changes.[13]

One might expect that the smaller values of J for the Mn(II) complexes than for the copper or vanadyl complexes would indicate that exchange had a much smaller impact on the nitroxyl EPR spectra of the former than of the latter. However, the decrease in the impact on the nitroxyl lines is not nearly so great as might be expected on the basis of the decrease in J. Interaction with an $S = {}^1/_2$ metal splits each nitroxyl line into a doublet with a separation of J. Interaction with an $S = {}^5/_2$ metal splits each nitroxyl line into a sextet with the spacing between adjacent lines equal to J and a total spread of the nitroxyl lines of $5J$. Thus, a decrease in J by a factor of 10 is only a decrease of a factor of 2 in the spread of the nitroxyl lines. Furthermore, since the manganese g value is so close to the nitroxyl g value, a small value of J is sufficient to cause significant mixing of the manganese and nitroxyl wave functions and relaxation behavior. Thus, even a small exchange interaction causes a large increase in the nitroxyl line width.

Implications of the Observations of Exchange Splitting with Respect to the Applicability of the Leigh Model to Manganese–Nitroxyl Interactions. In 1970 Leigh proposed that the decrease in the amplitude of the EPR spectrum of a nitroxyl radical interacting with Mn(II) in a rigid lattice could be interpreted by a model which had two key assumptions.[7] First, it was assumed that exchange interaction was negligible and that only dipolar interaction was significant. Second, it was assumed that the Mn(II) relaxation rate was fast relative to the magnitude of the spin–spin splitting, and therefore an increase in the metal relaxation rate would result in a narrowing of the nitroxyl EPR signal. The results of the present study indicate that both these assumptions need further examination for many systems.

It has generally been assumed that because of the dependence of dipolar interactions on the electronic spin and the inverse dependence of exchange interactions on the number of unpaired electrons, the importance of dipolar interactions would increase and the importance of exchange interactions would decrease as the number of unpaired electrons increased.[8] For molecules that are tumbling rapidly in fluid solution the dipolar splitting is averaged to approximately zero, and the exchange splitting can be measured without interference from the dipolar splitting. Our results indicate that although the values of J are substantially smaller for Mn(II) than for $S = {}^1/_2$ metals, the impact of the exchange interaction on the nitroxyl EPR spectra is dramatic even for small values of J. Significant interaction can be observed through σ- or π-orbital pathways. Because the exchange interaction results in mixing of the Mn(II) and nitroxyl wave functions, the nitroxyl line widths are dependent on the extent of exchange interaction. Thus, exchange must be considered as a possible source of line broadening in Mn(II)–nitroxyl interactions.

The model discussed in ref 7 is specifically limited to the regime in which the metal relaxation rate T_1^{-1} is faster than the energy separation (in Hz) that results from the spin–spin interaction. It

(29) More, K. M.; Eaton, G. R.; Eaton, S. S. *Inorg. Chem.* **1983**, *22*, 934–939.
(30) Eaton, S. S.; More, K. M.; Sawant, B. M.; Boymel, P. M.; Eaton, G. R. *J. Magn. Reson.* **1983**, *52*, 435–449.
(31) Eaton, S. S.; Boymel, P. M.; Sawant, B. M.; More, J. K.; Eaton, G. R. *J. Magn. Reson.* **1984**, *56*, 183–199.
(32) Richardson, P. F.; Kreilick, R. W. *J. Phys. Chem.* **1978**, *82*, 1149–1151.
(33) Hay, P. J.; Thibeault, J. C.; Hoffmann, R. *J. Am. Chem. Soc.* **1975**, *97*, 4884–4899.

was pointed out that if the relaxation rate were slower than this value, resolved splitting would be observed.[7,34] In ref 7 it was estimated that the Mn(II) T_1 was about $0.6–1.5 \times 10^{-9}$ s or T_1^{-1} was $1.7–0.7 \times 10^9$ s^{-1}. These values would permit the model to be used for splittings up to 140 or 57 G, respectively.[35] More recently it was estimated that the T_1 for Mn(II) in a biological molecule was $>8 \times 10^{-9}$ s.[36] This value of T_1 would restrict the use of the model to splittings of less than 10 G (and to correspondingly long interspin distances).

The results obtained for the Mn(II) complexes of ligands I to XI support the proposal that the Mn(II) T_1 is relatively long. The observed spectra show spin–spin splittings which would not be observable if the Mn(II) relaxation rate were as fast as assumed in ref 7. Thus, it is evident that at least for some Mn(II) complexes the metal relaxation rate is too slow to permit use of the model in ref 7 to analyze Mn(II)–nitroxyl interactions.

Some consideration must be given to the potential generality of these results. Modulation of the metal zero field splitting (ZFS) is generally believed to make a significant contribution to metal relaxation processes.[37] Thus, relaxation rates are expected to increase as ZFS increases. The modulation of the ZFS can be due to molecular tumbling and/or motion of the ligands in the metal coordination sphere.[37] A metal with a large ZFS might still have a slow relaxation rate if tumbling were slow and the metal coordination environment were rigidly fixed.

Values of the ZFS parameters for a series of adducts of Mn(acac)$_2$ have been reported ranging from $D = 330$ G and $E = 95$ G for Mn(acac)$_2$py$_2$ to $D = 736$ G and $E = 0$ for Mn(acac)$_2$en.[38,39] In Mn(hfac)$_2$phen $D = 320$ G and $E = 55$ G, and in Mn(hfac)$_2$bpy $D = 850$ G and $E = 200$ G.[40] The frozen solution EPR spectra of Mn(tfac)$_2$py$_2$ and Mn(hfac)$_2$py$_2$ were consistent with a value of D in this range. However, the spectra were broad and indicated the existence of a distribution of values of D as has been observed for other Mn(II) complexes,[41,42] so it was not possible to determine a precise value of D. Values of D of this magnitude have been reported for Mn(II) in biological systems, for example, Mn(II) soybean agglutinin ($D = \sim 100$ G, $E = \sim 20$ G),[41] glutamine synthetase–Mn(II)–methionine sulfoxime–AMP ($D = 126–140$ G),[43] glutamine synthetase–Mn(II)–methionine sulfoximine ($D = 150$ G),[44] Mn^{II}ADP–creatine–creatine kinase–thiocyanate ($D = 200$ G, $E = 37$ G),[45] Mn^{II}ADP–creatine–creatine kinease ($D = \sim 200$ G),[46] adenosyl succinate synthetase–MnGDP–aspartate ($D = 220$ G, $E = 52$ G),[45] Mn(II) Ca(II) concanavalin A ($D = 232$ G, $E = 43$ G),[47] MnADP–formyltetrahydrofolate synthetase–tetrahydrofolate–formate ($D = 243$, $E = 47$ G),[45] rabbit muscle phosphoglucomutase ($D = \sim 250$ G),[48] Mn^{II}ADP–creatine–creatine kinase–formate ($D = 320$ G),[49] pyruvate kinase–Mn(II)–oxalate ($D = 331$ G, $E = 44$ G),[45] Mn^{II}ADP–creatine–creatine kinase–nitrate ($D = \sim 450$ G),[50] and Mn(II) ionophore A23187 ($D = \sim 300$ to ~ 500 G).[51] Thus, the values of D estimated for the complexes of I to XII are similar to those reported for some biological molecules. The tumbling rates of large macromolecules are slower than for small molecules, so to whatever extent molecular tumbling contributes to the metal relaxation rates in the complexes of I to XII, slower metal relaxation rates would be expected for larger molecules. The macromolecules could also prevent solvent accessibility to the Mn(II) coordination environment so that mechanism of modulating the ZFS might also be less effective than for the small molecules. For molecules with similar ZFS it appears more likely that the Mn(II) relaxation would be slower in a macromolecule than in a small molecule rather than faster. Thus, it might be argued that the limitations on the applicability of the Leigh theory may be more severe for some biological systems than for the molecules examined here. Further studies are underway of spin-labeled Mn(II) complexes in which the Mn ZFS is larger. These should help to determine the extent to which the Mn(II) relaxation rate changes as a function of ZFS and whether the Leigh model is applicable when the ZFS is larger.

Conclusion

Electron–electron spin–spin splitting has been observed in a series of spin-labeled complexes of Mn(II). The changes in the spin–spin coupling constant, J, as a function of the bond pathway between the metal and the nitroxyl parallel results obtained previously for vanadyl complexes of the same ligands. The values of J are about an order of magnitude smaller for Mn(II) ($S = {}^5/_2$) than for vanadyl ($S = {}^1/_2$). The observation of splitting indicates that the manganese relaxation rate is slow relative to the magnitude of the spin–spin splitting. This observation indicates that a basic assumption of a widely used model for interpreting Mn(II)–nitroxyl interactions in biological systems[7] is not valid for some Mn(II) complexes.

Acknowledgment. This work was supported in part by NIH Grant GM21156.

Registry No. VII, 91281-14-0; XIII, 91281-13-9; Mn(tfac)$_2$·I, 91280-91-0; Mn(tfac)$_2$·II, 91280-92-1; Mn(tfac)$_2$·III, 91280-93-2; Mn(tfac)$_2$·IV, 91280-94-3; Mn(tfac)$_2$·V, 91280-95-4; Mn(tfac)$_2$·VI, 91280-96-5; Mn(tfac)$_2$·VII, 91280-97-6; Mn(tfac)$_2$·VIII, 91280-98-7; Mn(tfac)$_2$·IX, 91280-99-8; Mn(tfac)$_2$·X, 91281-00-4; Mn(tfac)$_2$·XI, 91281-01-5; Mn(tfac)$_2$·XII, 91281-02-6; Mn(hfac)$_2$·I, 91281-03-7; Mn(hfac)$_2$·II, 91281-04-8; Mn(hfac)$_2$·III, 91294-44-9; Mn(hfac)$_2$·IV, 91281-05-9; Mn(hfac)$_2$·V, 91281-06-0; Mn(hfac)$_2$·VI, 91281-07-1; Mn(hfac)$_2$·VII, 91294-45-0; Mn(hfac)$_2$·VIII, 91281-08-2; Mn(hfac)$_2$·IX, 91281-09-3; Mn(hfac)$_2$·X, 91281-10-6; Mn(hfac)$_2$·XI, 91281-11-7; Mn(hfac)$_2$·XII, 91281-12-8.

(34) In ref 7 it was stated that doublets would be observed. This would only be the case for metals with $S = {}^1/_2$. More generally $2S + 1$ lines would be observed for a nitroxyl interacting with a metal with spin S.

(35) The arguments here are analogous to saying that the theory is applicable for metal relaxation rates faster than the rate at which two peaks coalesce in two site exchange. The peaks coalesce when $T_1 = 0.23/\delta\nu$.

(36) McLaughlin, A. C.; Leigh, J. S., Jr.; Cohn, M. *J. Biol. Chem.* **1976**, *251*, 2777–2787.

(37) Burlamacchi, L.; Martini, G.; Ottaviani, M. F.; Romanelli, M. *Adv. Mol. Relaxation Interact. Processes* **1978**, *12*, 145–186 and reference therein.

(38) O'Conner, C. J.; Carlin, R. L. *Inorg. Chem.* **1975**, *14*, 291–296.

(39) Mercati, G.; Morazzoni, F.; Naldini, L.; Seneci, S. *Inorg. Chim. Acta* **1979**, *37*, 161–168.

(40) Birdy, R. B.; Goodgame, M. *Inorg. Chim. Acta* **1979**, *36*, 281–288.

(41) Meirovitch, E.; Poupko, R. *J. Phys. Chem.* **1978**, *82*, 1920–1925.

(42) Tsay, F.-D.; Manatt, S. L.; Chan, S. I. *Chem. Phys. Lett.* **1972**, *17*, 223–226.

(43) Hofmann, G. E.; Glaunsinger, W. S. *J. Biochem. (Tokyo)* **1978**, *83*, 1769–1778.

(44) Villafranca, J. J.; Ash, D. E.; Wedler, F. C. *Biochemistry* **1976**, *15*, 544–553.

(45) Markham, G. D.; Rao, B. D. N.; Reed, G. H. *J. Magn. Reson.* **1979**, *33*, 595–602.

(46) Reed, G. H.; Cohn, M. *J. Biol. Chem.* **1972**, *247*, 3073–3081.

(47) Meirovitch, E.; Luz, Z.; Gilboa, A. J. *J. Am. Chem. Soc.* **1974**, *96*, 7538–7541. Meirovitch, E.; Luz, Z.; Kalb, A. J. *Ibid.* **1974**, *96*, 7542–7546.

(48) Reed, G. H.; Ray, W. J., Jr. *Biochemistry* **1971**, *10*, 3190–3197.

(49) Reed, G. H.; McLaughlin, A. C. *Ann. N. Y. Acad. Sci.* **1973**, *222*, 118–129.

(50) Reed, G. H.; Cohn, M. *J. Biol. Chem.* **1972**, *247*, 3073–3081.

(51) Puskin, J. S.; Gunter, T. E. *Biochemistry* **1975**, *14*, 187–191.